Journal of Materials Processing Tech. 271 (2019) 249–260

Contents lists available at ScienceDirect

Journal of Materials Processing Tech.

journal homepage: www.elsevier.com/locate/jmatprotec

A single-step fabrication approach for development of antimicrobial surfaces

Yukui Cai[a], Xichun Luo[a,*], Michelle Maclean[b,c], Yi Qin[a], Mark Duxbury[d], Fei Ding[a]

[a] Centre for Precision Manufacturing, DMEM, University of Strathclyde, UK
[b] Department of Electronic and Electrical Engineering, University of Strathclyde, UK
[c] Department of Biomedical Engineering, University of Strathclyde, UK
[d] Department of Surgery, Glasgow Royal Infirmary, UK

ARTICLE INFO

Associate Editor: A. Clare

Keywords:
Anti-bacterial surface
Silver nanoparticles
Laser ablation
Hybrid machining

ABSTRACT

In recent years, the increasing incidence of healthcare-associated infections and overuse of antibiotics have led to high demand for antimicrobial-coated medical devices. Silver nanoparticles (AgNPs) have attracted tremendous attention as a subject of investigation due to their well-known antibacterial properties. However, current physical and chemical synthesis methods for AgNPs are costly, time-consuming and not eco-friendly. For the first time, this paper proposes a novel single-step fabrication approach, named StruCoat, to generate antimicrobial AgNPs coated microstructures through hybridizing subtractive laser ablation and additive chemical deposition processes. This new approach can offer antimicrobial micro-structured silver coatings for medical devices such as surgical tools and implants. The StruCoat approach is demonstrated on 316 L stainless steel specimens structured by using nanosecond pulsed laser, while AgNPs are decomposed and coated on these microstructures from the micro drops of silver nitrate solution simultaneously generated by an atomizer. According to the experimental results, silver nitrate with a molarity of 50 mmol and jet to the stainless steel machined at 14 W are the best-operating conditions for chemical decomposition of drops of silver nitrate solution in this research and results in AgNPs with a mean size of 480 nm. Moreover, an investigation of the material microstructures of stainless steel surfaces processed by StruCoat shows significant reduction of material grain size (81% reduction compared to that processed by normal laser machining) which will help improve the fracture toughness and strength of the specimen. Antimicrobial testing also demonstrated that specimens processed by StruCoat exhibited excellent antibacterial properties with 86.2% reduction in the surface attachment of *Staphylococcus aureus* compared to the smooth surface. Overall, this study has shown StruCoat is a potential approach to prepare antimicrobial surfaces.

1. Introduction

Surgical site infections are one of the most devastating complications after surgical procedures. More seriously, with the increased use of antimicrobial drugs, the threat of antimicrobial resistance is significant and is increasingly being recognized as a global problem (Roca et al., 2015). Thus, the increasing incidence of healthcare-associated infections and overuse of antibiotics leads to the need for alternative strategies which can decrease antibiotic consumption, such as the development of antimicrobial medical devices.

Surface treatment of medical devices by coating with antibacterial agents is a promising solution. Currently, silver and its compounds are the most commonly used antibacterial materials, due to their strong, broad-spectrum antimicrobial effects against bacteria, fungi, and viruses (Li et al., 2010). Recently, silver nanoparticles (AgNPs) have received interest for antimicrobial applications as they can enter bacterial membranes and deactivate respiratory chain dehydrogenases to inhibit respiration and growth of microorganism (Li et al., 2010). Due to this, AgNPs are believed to have good potential for application in silver-based dressings and silver-coated medical devices without promoting microbial resistance (De Giglio et al., 2013). A variety of physical and chemical methods was developed to prepare AgNPs on biomaterial substrates. For physical methods, Cao et al. (2011) employed silver plasma immersion ion implantation process to embed AgNPs on titanium substrates. The prepared samples were extremely effective in inhibiting both *Escherichia coli* and *Staphylococcus aureus* strains while exhibiting noticeable activity in promoting propagation of the osteoblast-like cells (MG63). Echeverrigaray et al. (2016) prepared stainless steel specimens with silver atoms by ion implantation process at low energy (4 keV) on a reactive low voltage ion plating equipment. Ferraris et al. (2017) deposited silver nanocluster/silica composites onto AISI 304 L stainless steel via a radio frequency (RF) co-sputtering

* Corresponding author.
E-mail address: xichun.luo@strath.ac.uk (X. Luo).

https://doi.org/10.1016/j.jmatprotec.2019.04.012
Received 22 January 2019; Received in revised form 14 March 2019; Accepted 2 April 2019
Available online 03 April 2019
0924-0136/

deposition method. After one month of immersing in diverse food relevant fluids, these coated specimens showed a good property for the reduction of bacterial adhesion. However, the high cost and low efficiency of the above physical methods limited the industrial application of AgNPs.

Researchers have also resorted to wet chemical procedures to synthesize AgNPs on biomaterials. Inoue et al. (2010) prepared sodium titanate thin films with a porous network structure through the reaction of titanium samples with NaOH solutions, then immersed in CH_3CO_2Ag solution for 3 h to conduct silver ion exchange treatment. Soloviev and Gedanken (2011) employed ultrasound irradiation to deposit AgNPs on stainless steel from $AgNO_3$ solution, which comprised aqueous ammonia and ethylene glycol. Diantoro et al. (2014) used sodium borohydride, mercaptosuccinic acid and methanol to finish the reduction reaction of AgNPs from silver nitrate solution. Heinonen et al. (2014) applied sodium hydroxide, ammonia and glucose to prepare the superhydrophobic surface with AgNPs by sol-gel technology. Jia et al. (2016) presented a strategy of mussel-adhesive-inspired immobilization of AgNPs. Moreno-Couranjou et al. (2018) employed catechols to realize the reduction of silver nitrate to obtain AgNPs. Cao et al. (2018) used dopamine as a reducing reagent to manufacture AgNPs on 304 stainless steel in a weak alkaline aqueous solution. All the testing results illustrated that the existence of silver nanoparticles is essential for the antibacterial activity of silver-containing surfaces.

The current chemical synthesis methods are not environmentally friendly as they involved at least two different chemical reagents in the chemical reaction (De Giglio et al., 2013). Thus, how to reduce the participant types of chemical reagents, even only using silver nitrates, is another challenge for the chemical synthesis method from the viewpoint of sustainable chemistry.

In addition to the coating approach, research has also demonstrated that microstructures of certain geometries can reduce surface adhesion of bacteria. Ferraris et al. (2019) proved that microgrooves on titanium surfaces prepared by electron beam surface structuring technology help to reduce adhesion of bacteria. For instance, in surgical tools, ultrasharp knife-edges in combination with textured surfaces in the knife-tissue contact region could lead to significant reductions in forces and consequent tissue damage. The microstructures act as stores to realize immobilization and release of silver ions into the surgical point. In addition, microstructures will protect the AgNPs from detachment and wear when subjected to external forces. Thus, the synergistic effect of AgNPs and micro-structures will lead to even better antibacterial results (Jia et al., 2016).

In this research, an innovative StruCoat approach is proposed for the preparation of anti-bacterial microstructures with AgNPs coatings, through a single step process. It is a hybrid fabrication approach which combines laser ablation technology for micro-structuring, and laser-assisted thermal decomposition and deposition for synthesizing and coating AgNPs from silver nitrate ($AgNO_3$) solution simultaneously. The StruCoat approach offers advantages for the synthesis of "green" AgNPs. There is no requirement for reducing and stabilizing agents involved in the chemical reaction, so the type of chemical reagent is reduced. More importantly, it offers durable silver coated microstructured anti-bacterial surfaces. This paper will explore the mechanism of StruCoat and the effects of laser power and molarity of silver nitrate on the morphology of microstructures and the size of AgNPs. It will also evaluate the antimicrobial performance of specimens prepared by StruCoat.

2. The working mechanism of StruCoat and experimental setup

2.1. Work principle of StruCoat

The schematic of StruCoat is illustrated in Fig. 1. In this work, an ultrasonic atomizer was used to produce micro/nano drops of $AgNO_3$ from liquid based on vibrating piezo crystal due to its robustness and capability of working at low pressure (Gaete-Garretón et al., 2018). As shown in Fig. 1, micro liquid drops of aqueous solutions of $AgNO_3$ emerging from the ultrasonic atomizer are transported to the nanosecond pulsed laser ablation zone. Laser heating will cause the melting and even gasification of stainless steel. The vapour and plasma pressure will result in the partial ejection of the molten materials from the cavity and formation of surface debris. The recast layer is formed as the thermal energy rapidly dissipates into the internal material (Wang et al., 2018). During the laser-materials interaction, the laser ablation zone is in a high-temperature state, so the adherent $AgNO_3$ drops are thermally decomposed to AgNPs and deposited on the surface continuously.

2.2. Mechanism of decomposition and deposition of AgNPs

Heating will result in decomposition of most metallic nitrates into their corresponding oxides. However, the decomposition product of silver nitrate is elemental silver as silver oxide has a lower decomposition temperature than silver nitrate. Qualitatively, decomposition of silver nitrate is tiny under the melting point, but it is becoming increasingly apparent at about 250 °C, while total decomposition will take place at 440 °C (Stern, 1972). The chemical decomposition equation of silver nitrate can be described as:

$$2\ AgNO_3(liquid) \rightarrow 2\ Ag(solid) + O_2(gas) + 2\ NO_2(gas) \quad (1)$$

In this research, an ultrasonic atomizer with a diameter of 20 mm and frequency (f) 113 KHz was employed in the experiments. In the process of ultrasonic atomization, a square wave pattern would be formed on the surface of the liquid when approaching resonance

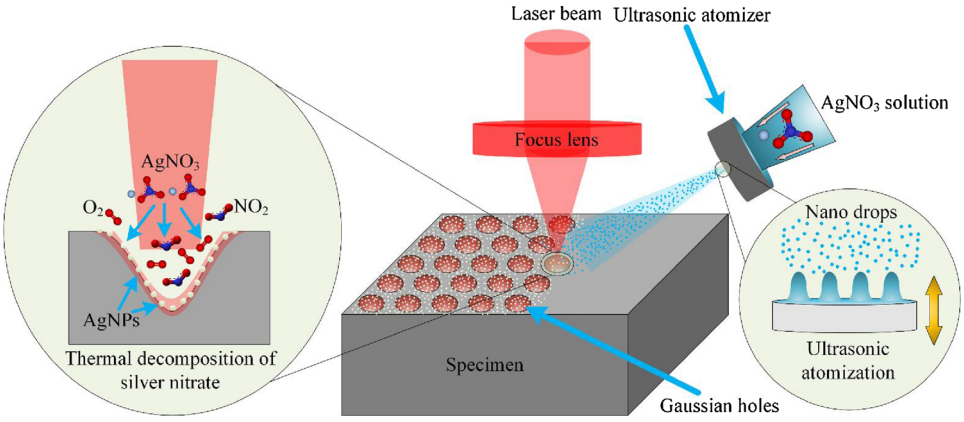

Fig. 1. Schematic illustration of StruCoat.

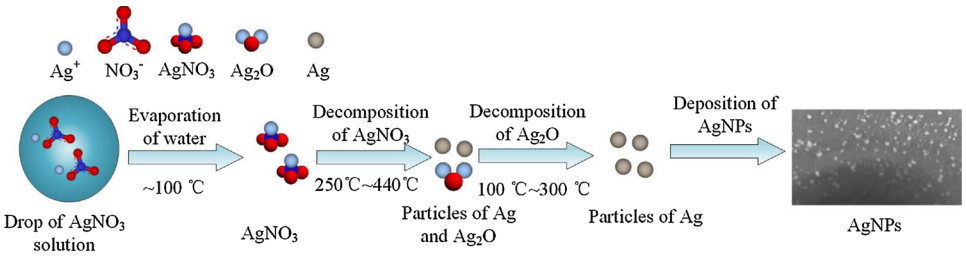

Fig. 2. Chemical reaction process of AgNPs.

frequency of atomizer. Micro drops were ejected from square waves crests, thus, its diameters were strongly correlated to the wavelength of the wave (Dobre and Bolle, 2002). The wavelength λ can be expressed as:

$$\lambda = \left(\frac{16\pi\sigma}{\rho_L f^2}\right)^{\frac{1}{3}} \tag{2}$$

where σ is the surface tension of liquid, ρ_L is the density of liquid, and f is the frequency of atomizer.

The most probable diameter of drops, D_L, can be calculated by Eq. (3) (Šarkovic and Babovic, 2005).

$$D_L = C^{-1}\lambda \tag{3}$$

where C is the experimentally coefficient confirmed by (Pohlman, Reimar, 1965). According to the recommendation by Šarkovic and Babovic (2005), C = 4 is used in this research. Thus, the most probable probability diameter of drops D_L is 8.2 μm, when σ = 0.073 N/m, ρ_L = 1000 Kg/m^3, and f = 113KHz.

Then, the most probable diameter of silver particle D_{Ag} can be calculated by the Eq. (4).

$$D_{Ag} = \frac{1}{4}\left[\left(\frac{2\pi\sigma C_{Ag} M_{Ag}}{\rho_L \rho_{Ag} f^2}\right)\right]^{\frac{1}{3}} \tag{4}$$

where, C_{Ag} is the molarity of silver ions, which is equal to the molarity of silver nitrate solution. M_{Ag} is the molar mass of silver, which is 107.8682 g/mol, and ρ_{Ag} is the density of silver, which is 10,530 kg/m^3.

Fig. 2 illustrates the whole chemical reaction processes. The water starts to evaporate when drops of silver nitrate solution make contact with the high-temperature molten layer. Solid silver nitrate crystals are formed on the surface, but they start to decompose to silver oxide and silver when the temperature is higher than 250 ℃ and decomposes completely when the temperature is above 440 ℃ (Stern, 1972). In addition, the silver oxide is continuously decomposed to silver if the temperature is still higher than 300 ℃. In the laser machining process, the absorption of laser energy leads to a rapid increase of local temperature, the maximum temperature realized 3500–14500 K (Thorslund et al., 2003), which is higher than the vapour temperature (3135 K for iron) of stainless steel. This temperature is much higher than the decomposition temperature of silver nitrate; so, there is sufficient thermal energy to finish the decomposition reaction as shown in Fig. 2. Then, the AgNPs deposit on the surface during the solidification of the molten materials in the laser ablation zone.

2.3. Materials and experimental setup

The AISI 316 L stainless steel plates (6 mm × 6 mm × 2 mm) were used as the experimental specimens in this research. Before laser machining, the stainless steel plates were machined by a flat end mill (with a diameter of 6 mm), as described by (Cai et al., 2018), giving a surface roughness (Sa) of about 0.2 μm. Silver nitrate (Alfa Aesar) and deionized water were used to prepare chemical solutions with different molarities of 25–200 mmol/L.

Fig. 3 (a) shows the hybrid ultra-precision machine used for experiments. The machine contains a nanosecond pulsed fibre laser which has a central emission wavelength of 1064 nm. The laser source has a nominal average output power of 20 W and its maximum pulse repetition rate is 200 kHz. An ultrasonic atomizer was employed to generate micro liquid drops as shown in Fig. 3(b). This research will

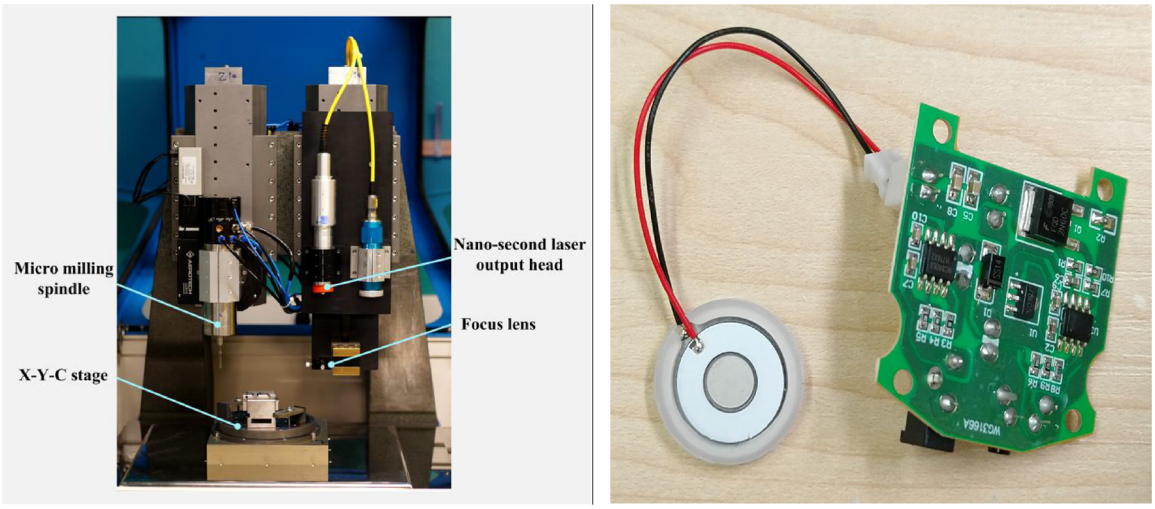

(a) (b)

Fig. 3. Experimental setup of StruCoat (a) Hybrid Precision machine used for laser machining process (b) Ultrasonic atomizer used to generate micro drops.

Table 1
Operational conditions used to evaluate the effect of laser power on the synthesis of AgNPs.

Laser power (W)	Pulse repetition rate	Feed rate (mm/min)	Duration time (S)	Pitch (μm)	Molarity of $AgNO_3$ (mmol/L)
2, 8, 14, 20	100K	200	0.4	90	50

Table 2
Operational conditions used to evaluate the effect of molarity of silver nitrate on the synthesis of AgNPs.

Laser power (W)	Pulse repetition rate	Feed rate (mm/min)	Duration time (S)	Pitch (μm)	Molarity of $AgNO_3$ (mmol/L)
14	100K	200	0.4	90	25, 50, 100, 200

investigate the effect of laser power and molarity of $AgNO_3$ on the surface topography and the size of AgNPs. Details of the operational conditions for the two experiments are shown in Tables 1 and 2.

2.4. Post-processing and characterization

All specimens were cleaned ultrasonically with deionized water, acetone and ethanol for 10 min to remove any organics on the surface before and after the experiments. Then, these specimens were dried in an oven at 100°C for 20 min. The surface chemistry and the morphology of laser structured Gaussian holes and deposited AgNPs were characterized by scanning electron microscopy (SEM) and X-ray diffraction (XRD).

2.5. Antimicrobial activity testing

Antibacterial experiments were implemented to assess the susceptibility of three different kinds of specimens to bacterial attachment and biofilm growth; (i) smooth, (ii) laser ablated and (iii) specimens fabricated by StruCoat. Samples were cleaned before each experiment using 70% ethanol to remove any contaminant bacteria already on their surface.

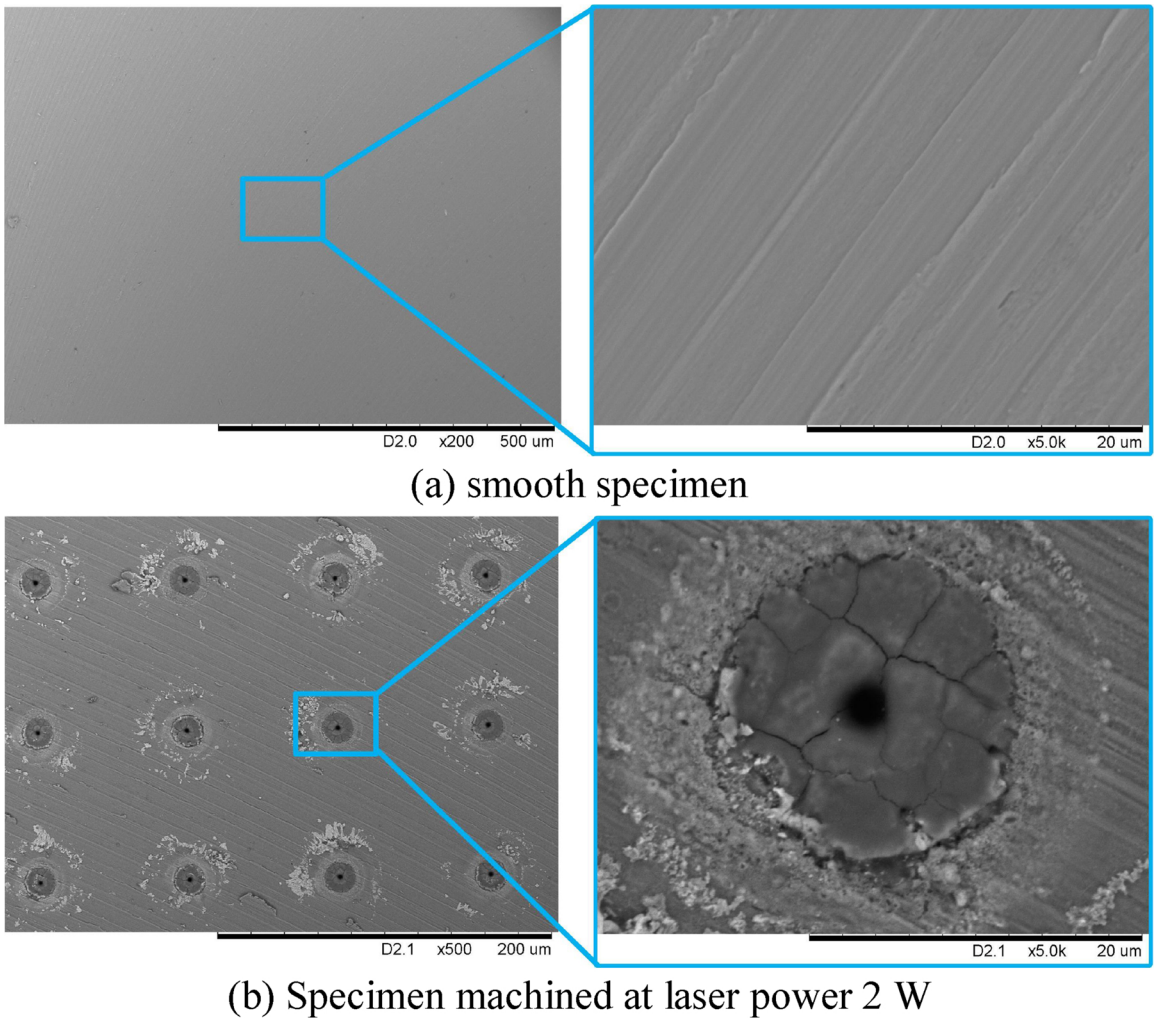

Fig. 4. SEM image (left) and high-magnification image (right) of Specimens manufactured by StruCoat under different laser power. Samples are (a) smooth; and machined at laser powers of (b) 2 W; (c) 8 W; (d) 14 W; (e) 20 W.

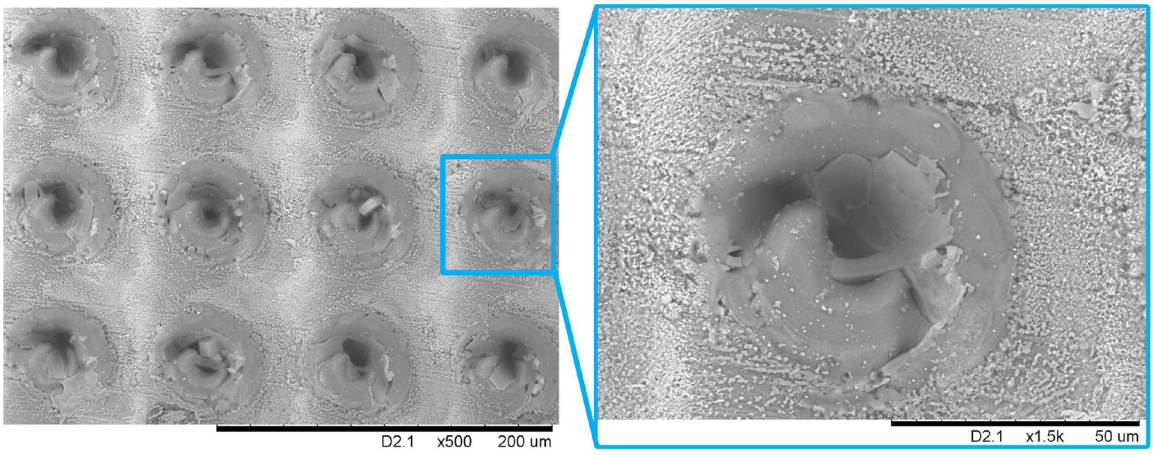

(c) Specimen machined at laser power 8 W

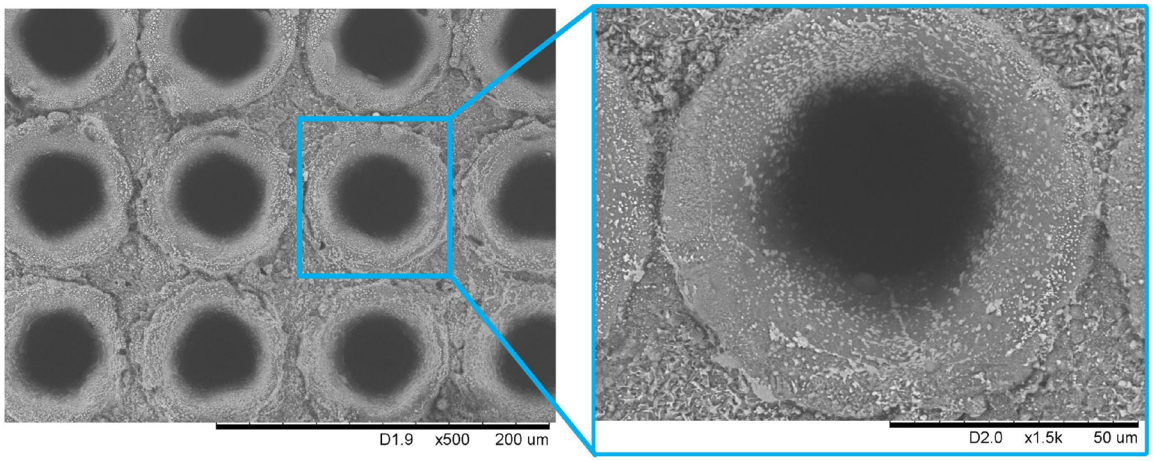

(d) Specimen machined at laser power 14 W

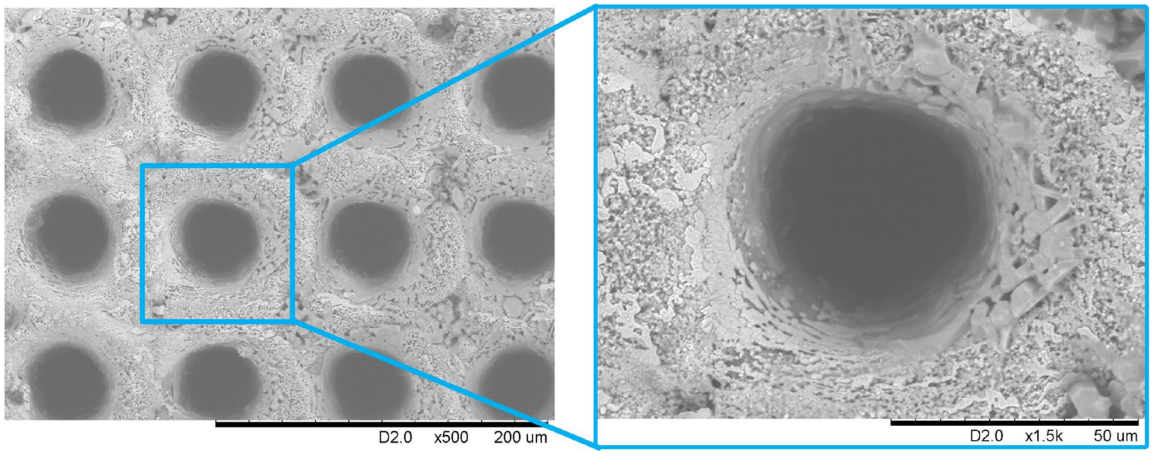

(e) Specimen machined at laser power 20 W

Fig. 4. (*continued*)

The bacteria used in all experiments was *Staphylococcus aureus* (NCTC 4135) and was selected as it is widely associated with commonly contracted medical device-related infections (Tong et al., 2015). *S. aureus* was cultured in 100 ml nutrient solution (Oxoid Ltd, UK) for 18 h at 37 °C with a rotational speed of 120 rpm. Post-incubation, the bacterial culture was centrifuged at 3939 × g and the pellet resuspended in phosphate buffered saline (PBS; Oxoid Ltd, UK), before being serially diluted to a concentration of 10^4 CFU/ml for experimental use.

Stainless steel specimens were immersed in 5 ml 10^4 CFU/ml bacterial suspension in multiwell culture plates and incubated at 37 °C for 24 h to permit attachment and subsequent biofilm formation (Vollmerhausen et al., 2017). Following incubation, the samples were rinsed in sterile PBS to remove any excess planktonic bacteria not attached to the biofilm. The samples were then placed into 9 ml PBS, and the surface-attached bacteria were physically removed from the surfaces using the following methodology: 10 s manual agitation followed

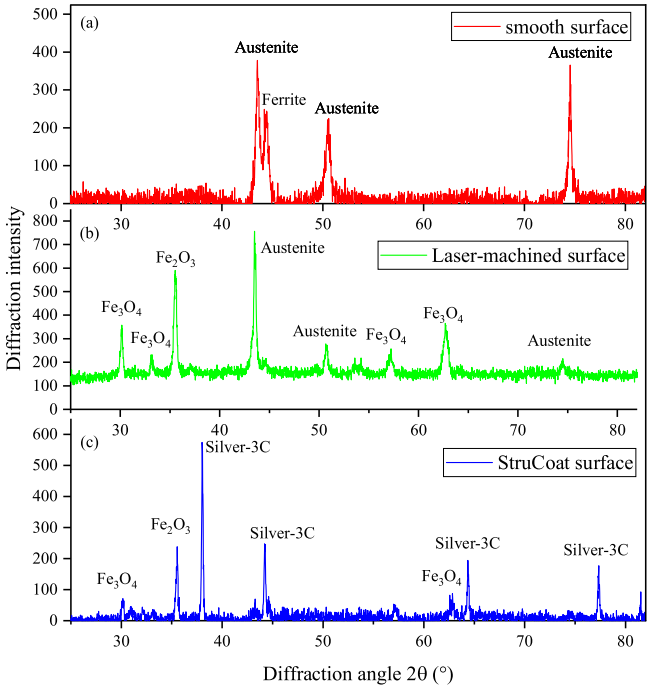

Fig. 5. X-ray diffraction pattern of 316 L stainless steel (a) smooth surface and (b) laser-machined surface (c) StruCoat surface.

by 300 s in an ultrasonic bath followed by a further 10 seconds manual agitation. This process facilitated the release of the attached bacteria from the surface into the PBS 'capture fluid', with this fluid then being serially diluted and samples spread plated onto nutrient agar (Oxoid Ltd, UK) (n = 3). Plates were incubated at 37 °C for 24 h, and results enumerated as CFU/ml.

3. Results and discussion

In the laser ablation process, the material was removed from the substrate surface due to high peak power results in thermal energy higher than breakdown thresholds of material which would lead to material melting, ablation and vapour generation. The thermal energy also helped to form the high-temperature zone around the laser radiation area. The thermal decomposition of silver nitrate to silver particles relied on the heat generated in the laser ablation process. Thus, the size of microstructure and AgNPs could be tightly controlled by the laser power and molarity of silver nitrate. This section will analyze the influence of the above factors.

3.1. The effect of laser power on the morphology of AgNPs and microstructures

Fig. 4 shows the SEM images of the smooth surface and laser-ablated microstructures under different laser powers but at constant molarity of silver nitrate of 50 mmol/L. The increasing size of laser ablated microstructures was observed with the increase of laser power. The increased diameter of laser ablated holes and the thickness of casting layers is the result of molten metal flow driven by surface tension and recoil pressure formed by the evaporation (Zhou et al., 2016). Fig. 4(b)–(e), shows all specimens contained a certain amount of silver particles deposited on the surfaces. The possession of silver nanoparticles was further confirmed by XRD analysis results shown in Fig. 5.

At the laser power of 2 W, the heat dissipates quickly, so micro drops of silver nitrate have a very short time period to decompose to AgNPs. The theoretical diameter of liquid drops calculated by Eq. (3) is around 8.2 μm. However, the obtained maximum diameter of the microstructures in the experiment was approximately 20 μm at the laser power of 2 W. This indicated that the droplets have less probability falling in the laser ablated high-temperature area. When the laser power increased to 8 W, the maximum diameter of microstructure reached 50 μm. Some AgNPs were also formed on microstructures due to the high temperature of the molten layer. Fig. 4(c) and (d) show that more AgNPs were formed at a laser power of 14 W than 8 W. The diameter and depth of the melt pool increased with the increase of laser power as more energy was transferred into the heat-affected zone (HAZ). The sputtering area was formed at 14 W due to the vertical movement of liquid during irradiation caused by the vapour flow that expands in the Gaussian hole. As a result, AgNPs were deposited on both the spatter area and Gaussian holes. However, the flake-like silver started to form on the microstructures when laser power further increased to 20 W.

The thermal stress accumulation increased with the increase of laser power. This explained the increased quantity of AgNPs from lower to high laser powers. At the low laser power of 4 W, not enough accumulated thermal stress and physical space was generated for the silver nitrate to finish the decomposition process. However, when the laser power increased to 20 W, the laser ablated area was overheated. The excess heat energy led to a longer cooling time, so much more silver drops participated in the chemical reduction. These silver particles accumulated and formed silver particles with large dimensions. On the other hand, the evaporation and sputtering phenomenon would be enhanced significantly under high laser power, which had a negative effect on the deposition of AgNPs. Therefore, overheating would not beneficial for growing more AgNPs on the laser-ablated structures. Proper thermal energy would be necessary for the deposition of AgNPs. It is also known that the uniform distribution of AgNPs is beneficial to anti-bacterial properties (Gurunathan et al., 2014). As such, specimens processed at the laser power 14 W had the most homogeneous size distribution of the AgNPs, and thus it was deemed the best result for deposition of AgNPs on the laser ablation zone.

The XRD patterns of the smooth surface, laser-machined surface and StruCoat surface of 316 L stainless steel are shown in Fig. 5. In Fig. 5(a), there are three sharp diffraction peaks corresponding to the XRD pattern of austenite and one peak for ferrite. For the laser-machined surface, it was found that austenite, Fe_3O_4 and Fe_2O_3 were recognized on the XRD pattern. In Fig. 5(c), the presence of pure silver is confirmed by the diffraction peaks at 2θ = 38.2°, 44.4°, 64.6° and 77.5° on StruCoat surface, which correspond to scattering from (111), (200), (220) and (311) planes of pure silver. Thus, the XRD pattern in Fig. 5(c) proves the existence of AgNPs.

3.2. The effect of silver nitrate molarity on the synthesis of AgNPs

The molarity of silver nitrate is another critical processing parameter in StruCoat for deposition of AgNPs. In this section, different molarities of silver nitrate, as listed in Table 2, were employed to conduct the experiment.

Fig. 6 showed the morphologies of microstructured surfaces processed by StruCoat at different molarities of silver nitrate solutions varying from 25 mmol to 200 mmol, while the laser power was fixed at 14 W. For the specimens which employed 25 mmol, 50 mmol and 100 mmol silver nitrate solutions, the AgNPs could be clearly observed. The distribution density of AgNPs was significantly higher while the molarity of the silver nitrate solution was 50 mmol. The density of silver ions increased with the increase of molarity of silver nitrate solution. Low molarity of silver ions required less thermal energy in the chemical reduction process, thus, the excess heat leads to AgNPs being evaporated furtherly. This explains the increase in distribution density of AgNPs while the molarity of silver nitrate solution was increased from 25 mmol to 50 mmol. However, when the molarity of silver nitrate solution increased to 100 mmol, aggregation and clumping of the AgNPs were observed. Some adjacent AgNPs started to weld together, with some silver bars starting to appear on the microstructure. There

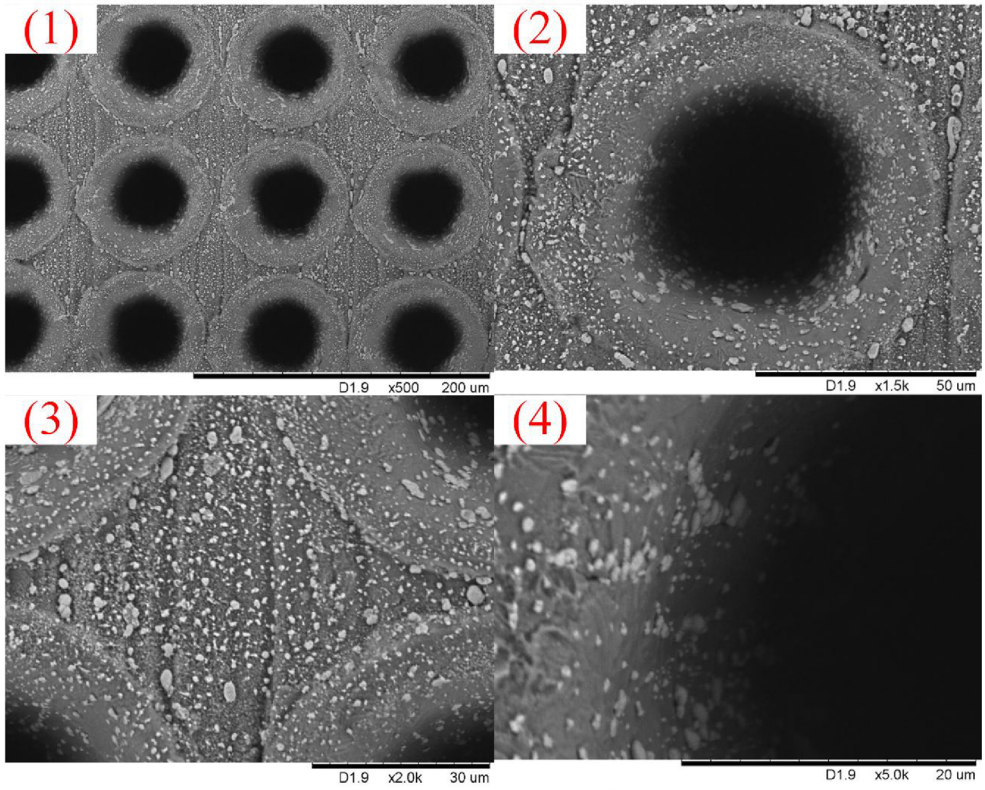

(a) 25 mmol solution of silver nitrate

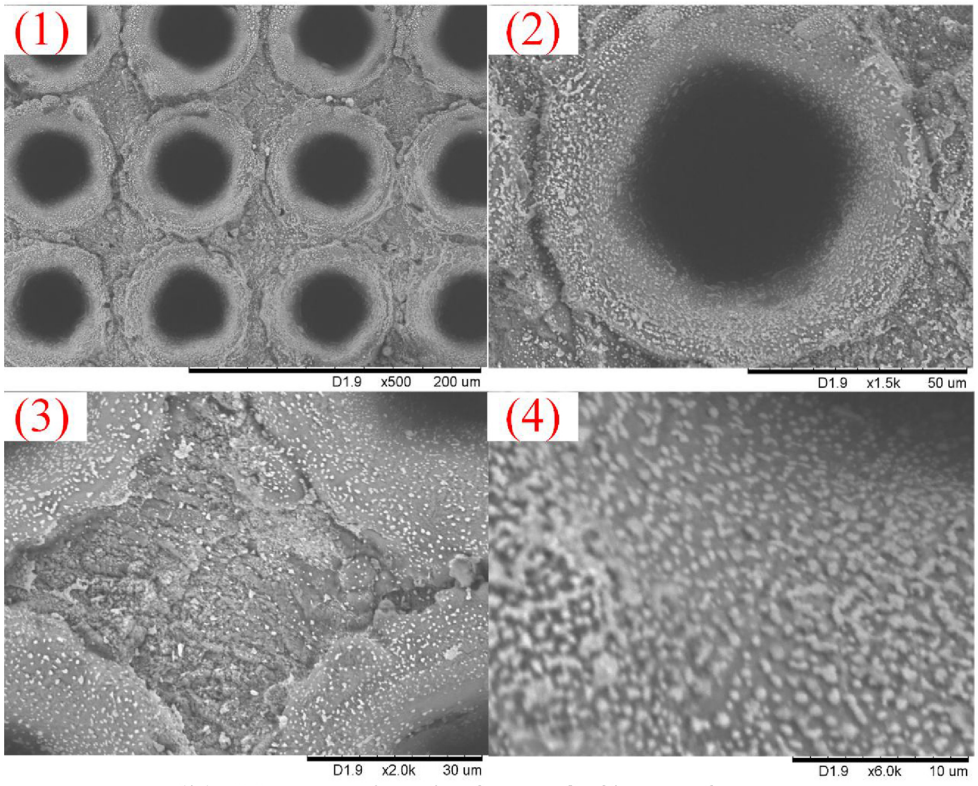

(b) 50 mmol solution of silver nitrate

Fig. 6. Low (×500) and high (×1.5–6.0k) magnification SEM images of StruCoat processed microstructured surfaces with different molarities of silver nitrate: (a) 25 mmol; (b) 50 mmol; (c) 100 mmol; (d) 200 mmol. Images labelled (1) were low magnification (×500) and (2)–(4) were high magnification (×1.5–6.0k). Arrows on images indicate silver particles.

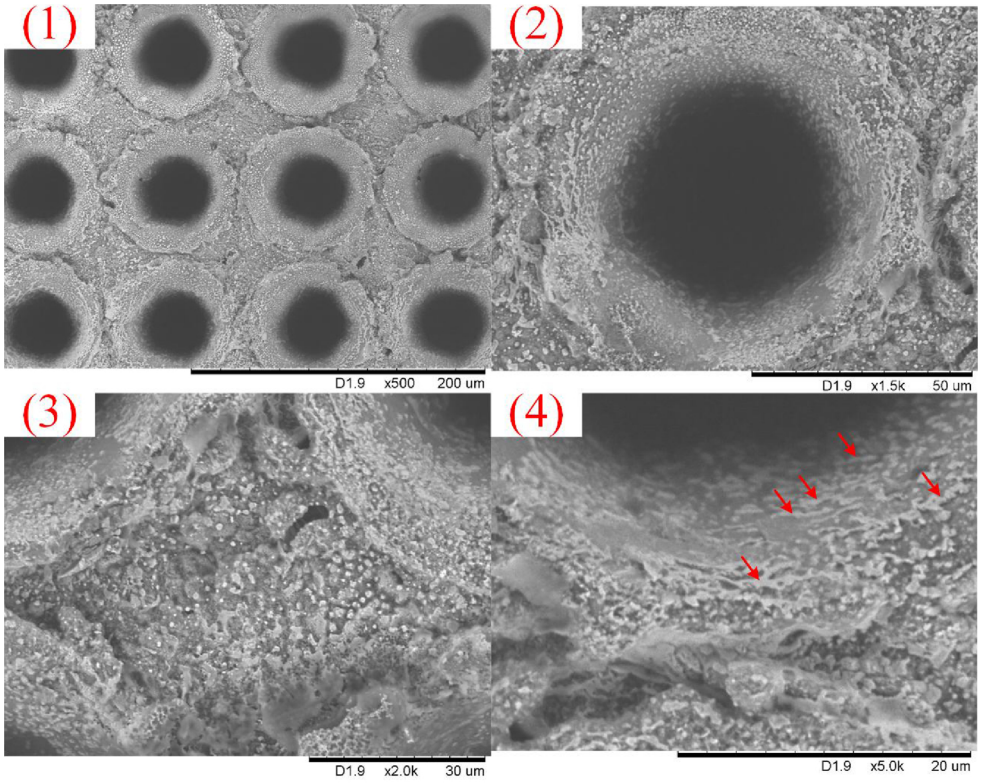

(c) 100 mmol solution of silver nitrate

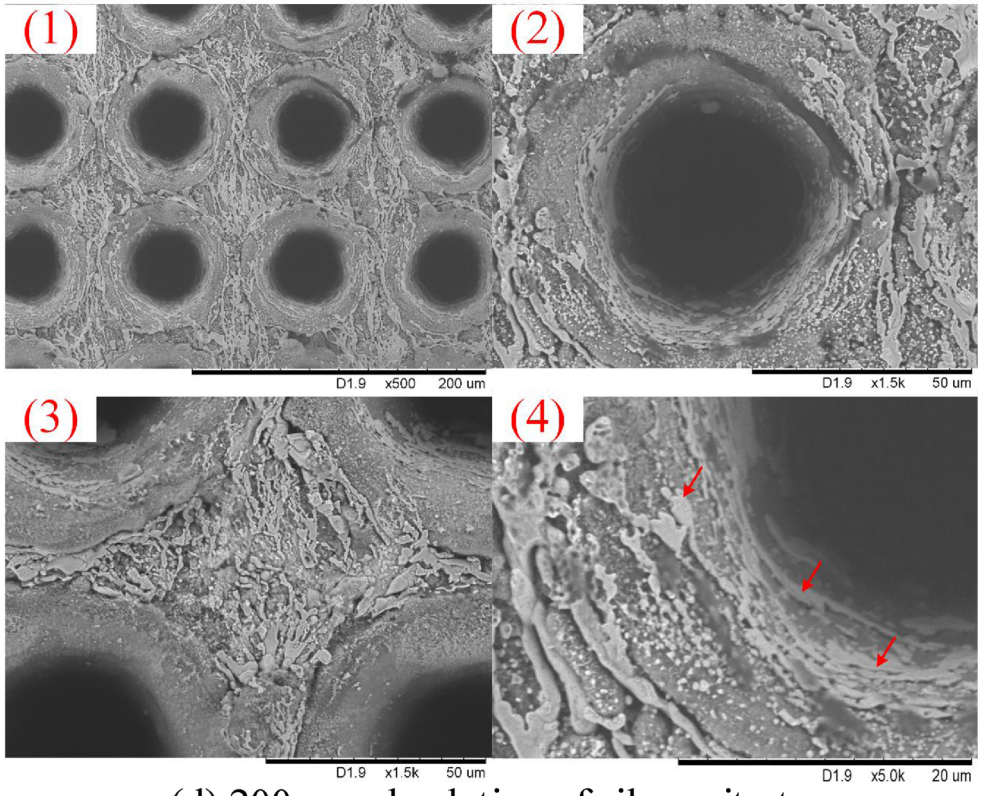

(d) 200 mmol solution of silver nitrate

Fig. 6. (*continued*)

were a number of reasons which could explain these observations. Firstly, the silver nitrate solution of higher molarity required more energy to finish thermal decomposition reaction, resulting in insufficient heat energy for evaporation of the silver particles. Secondly, the surface tension and density of drops of silver nitrate increased with the increase of molarity of silver nitrate, thus the adjacent drops were more possibly connected to each other when they were deposited on the microstructure and formed larger drops. Thirdly, the high molarity of

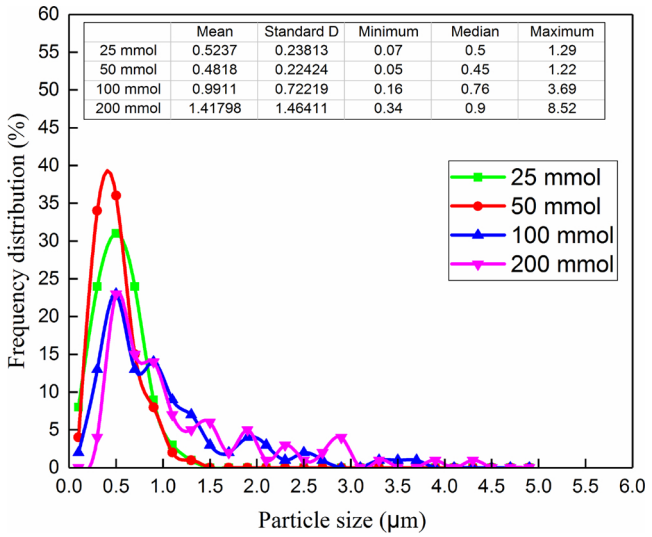

Fig. 7. Size distribution of AgNPs for specimens machined with different molarity of silver nitrate.

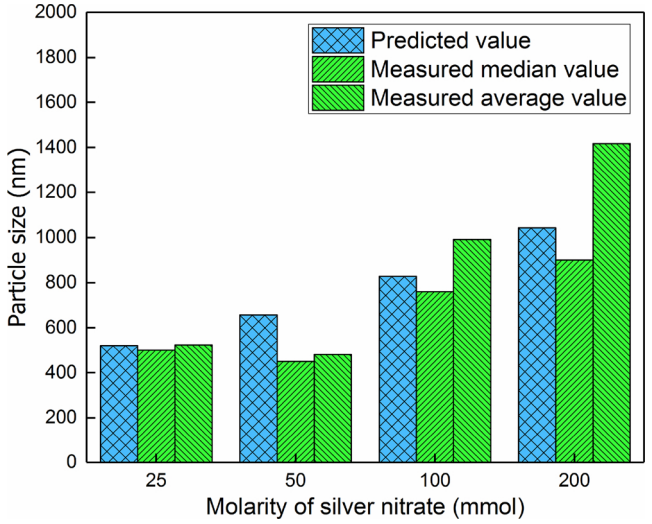

Fig. 8. Comparison between predicted and measure particles size.

silver ions in every drop could have resulted in more silver being deposited on the substrates. As shown in Fig. 6(d), the aggregation and clumping of the AgNPs became more significant when the molarity of silver nitrate solution increased to 200 mmol.

The size distribution of AgNPs was shown in Fig. 7. The length of 100 particles with a clear profile was measured manually by image processing software (Nano Measurer 1.2.5) based on the SEM image (4) in Fig. 6. The size of AgNPs was found to be dependent on the molarity of the silver nitrate solution. At low molarity (25 mmol and 50 mmol), the mean particle size of microspheres was 400–600 nm. At high molarity (100 mmol and 200 mmol), the mean particle size reached micron level. Nevertheless, the particle size of 500 nm had the maximum proportion for all the specimens. In addition, a low standard deviation indicated that the data points tended to close to the mean value, while a high standard deviation indicated that the data points were spread out over a wider range of values. Thus, the best molarity was 50 mmol as it led to specimen with a minimum mean particle size of 480 nm and minimum standard deviation of 224 nm. This indicated that too high a molarity was not beneficial for growing more silver particles in nanoscale on the laser-ablated structures, and applicable molarity of silver nitrate solution would be necessary for the generation of AgNPs with uniform distribution in the average size.

Comparison between the predicted and measured diameter of silver particles is shown in Fig. 8. The predicted value was closer to the measured median value than the average value. In theory, with the increase of molarity of silver nitrate, the predicted particles size increased gradually due to the increased silver included in the micro drops. The experimental results showed the same tendency except at 50 mmol. It obtained similar particle sizes of approximately 500 nm at molarities of 25 and 50 mmol in experiments. Thus, the theoretical and experimental results indicated that it was not necessary to employ silver solutions with high molarity as it could lead to the increased size of deposited particles.

Fig. 8 Comparison between predicted and measure particles size

In order to observe the interface between AgNPs and the substrates of stainless steel Focused Ion Beam (FIB) milling was used to make a cross-section on the StruCoat processed surfaces. Fig. 9 shows SEM images of the subsurface topography. It could be observed that the AgNPs were firmly connected with the stainless steel after the wielding effect in the laser ablation process, and this helps to attain the high strength of interfacial bonding.

3.3. Material microstructures of StruCoat processed substrates

During the laser machining process, the rapid heating and cooling lead to modification of material microstructure. The laser machining heat affected zone (HAZ) is defined as the area that has not melted but has undergone thermal induced microstructural modification by laser pulses (Al-Mashikhi et al., 2011). This section will investigate the cross-sectional material microstructure of HAZ of 316L austenitic stainless

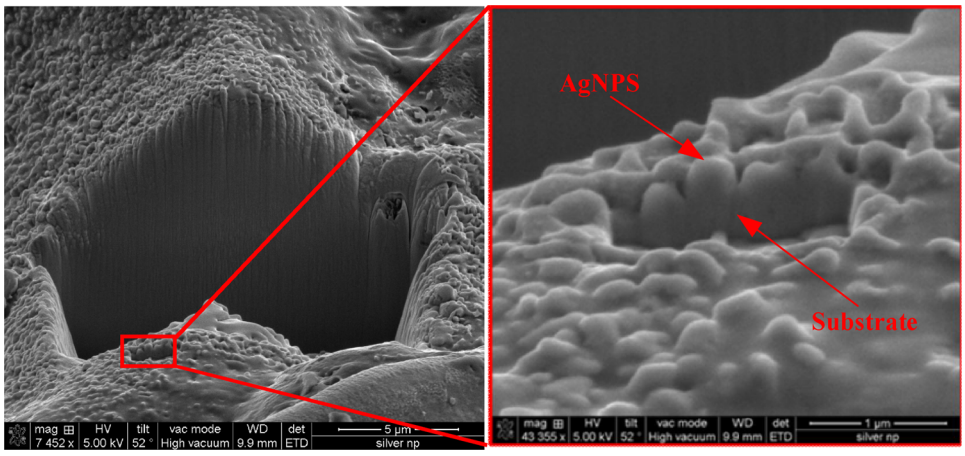

Fig. 9. Whole image of FIB processed areas (Left) and magnified image of the cross-section (Right).

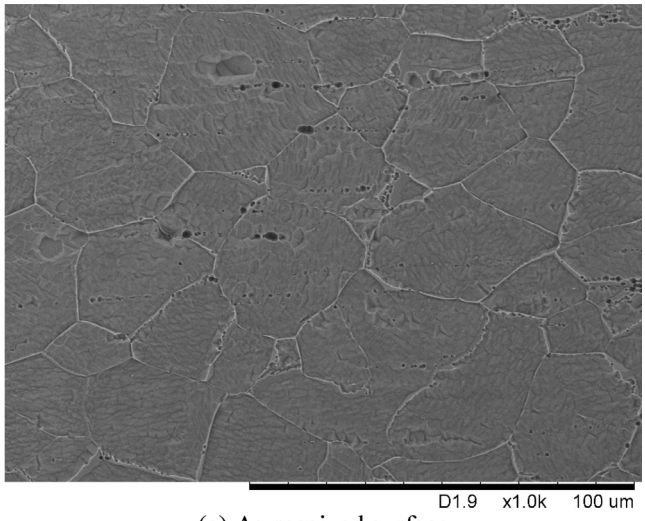

Fig. 10. SEM images (×1.0k) of cross-sections of stainless steel surfaces: (a) unprocessed, (b) processed by laser machining, (c) processed by StruCoat.

steel in the traditional laser machining process and the StruCoat process. Metallographic polishing methods were used to etch cross-sections of specimens in order to evaluate the changes to substrate structures.

SEM images of the metallographic structure of stainless steel surfaces (unprocessed, processed by laser machining, and processed by StruCoat) are shown in Fig. 10. The linear line intercept method was employed to measure grain size. The average grain sizes after laser machining process and StruCoat were about 9.3 μm and 4.5 μm, while the average size of the original grain in the as-received 316L stainless steel was about 24.6 μm. The significant grain size refinement was due to the laser reversion annealing through the intense heat input during the laser machining process. As a result, the grain refinement effect would lead to an increase in both material strength and fracture toughness. More importantly, the specimen had even higher cooling rates in StruCoat than in laser machining due to the evaporation of the aqueous solution, which resulted in a further decrease of grain size (81% reduction).

In addition, it could be clearly seen from Fig. 10(b) that the depth of the HAZ subjected to the laser machining process was about 97 μm, while the depth of HAZ in the StruCoat was about 62 μm. The reduced depth of HAZ in StruCoat was also due to the increased cooling rate in StruCoat.

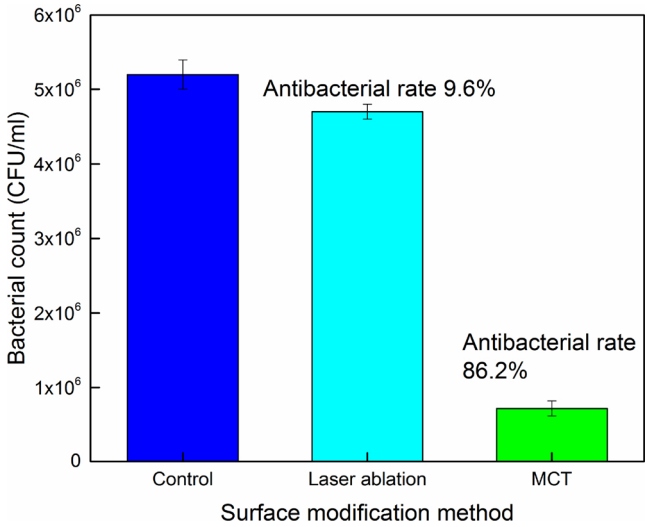

Fig. 11. Bacterial attachment and biofilm formation on StruCoat modified stainless steel surfaces. Results on smooth and laser ablated surfaces are included as a comparison (n = 3 ± standard deviation).

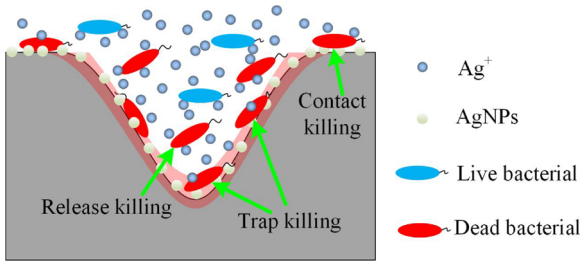

Fig. 12. Antibacterial mechanism of structured specimens coated with AgNPs (Jia et al., 2016).

3.4. Antibacterial evaluation of StruCoat

In this study, the antibacterial capabilities of the two stainless steel specimen processed by laser ablation and StruCoat were evaluated after 24 h cultivation with bacterial contamination. A smooth stainless steel specimen with no surface modifications was included as a comparative control. Results showed that specimens machined by laser ablation and StruCoat both demonstrated reductions in bacterial attachment and biofilm formation compared to the unmodified control, as shown in Fig. 11. Specimens processed by StruCoat exhibited a significantly greater reduction in bacterial attachment than laser ablated specimens

with a total decrease in bacterial count of 86.2% compared to the unmodified material, thus, the coating of AgNPs was critical for enhancing the antimicrobial capabilities of specimens manufactured by StruCoat. The slight antibacterial activity evidenced by the laser-ablated specimens without AgNPs (9.6% reduction in surface contamination) can likely be attributed to the generation of iron oxide during the laser ablation process; an effect which was documented in a study by Fazio et al. (2016).

Jia et al. (2016) explored the synergistic effect of AgNPs and microstructures, and proved that microstructures had a special antibacterial mode named “trap & kill”. Fig. 12 illustrates the possible sterilize modes engaged in the antibacterial process. First, the released silver ions from AgNPs killed some bacteria before it contacts with the surface, termed ‘release killing’. After the silver ion treatment, the bacterial membrane interacted with silver ions and resulted in cytoplasmic membrane shrinking and damage (Dakal et al., 2016). Secondly, some bacterial kill would attribute to direct contact with silver particles, termed ‘contact killing’. The accumulation of AgNPs in the bacterial membrane led to a significant increase in permeability, which results in the death of bacteria (Sondi and Salopek-Sondi, 2004). More importantly, bacterial cells with a negative charge would be introduced into the microstructures of the surfaces, causing binding with AgNPs via electrostatic attraction, and these were then killed through the contact killing mechanism. In addition, the microstructures could act simultaneously as storage pockets of AgNPs to attain sustainable release of silver ions, protecting AgNPs from friction-induced particle detachment. In terms of the significant antimicrobial effects observed in the present study, further work is required to determine the exact mechanism of action, and correlate with that of other studies using AgNPs such as that of Jia et al. (2016).

4. Conclusions

A single-step fabrication approach (named as StruCoat was proposed for the first time in this paper to generate antimicrobial microstructures coated with AgNPs on 316 L stainless steel. StruCoat laser ablation was used to generate microstructures, while micro drops of silver nitrate solution were delivered to the laser ablation zone to decompose and coat AgNPs onto microstructures by using the thermal energy generated in laser ablation process. The laser power and molarity of silver nitrate were identified as major control parameters for StruCoat. Experimental studies showed that silver nitrate with a molarity of 50 mmol at the laser power of 14 W – which resulted in AgNPs with a mean size of 480 nm – was the best processing condition for chemical decomposition of silver nitrate micro drops in this research.

StruCoat is an eco-friendly process due to the non-requirement of reducing and stabilizer agents, and only silver nitrate is required in the decomposition process. In addition, the microstructures could also act as storages for AgNPs to attain sustainable release of silver ions. AgNPs would mostly distribute at inner of the microstructures, thus, microstructures could provide protections to AgNPs to avoid friction-induced particle detachment. In addition, StruCoat would help increase the cooling rate of the substrate in the laser machining process and resulted in the significant decrease of material grain size (by 81%). Decreasing grain size will increase material strength and fracture toughness. Antimicrobial efficacy testing also demonstrated the enhanced antibacterial properties of StruCoat, with 86.2% anti-bacterial rate against *Staphylococcus aureus*, compared to unmodified samples, in the present study.

Data statement

All data underpinning this publication are openly available from the University of Strathclyde KnowledgeBase at https://doi.org/10.15129/af048a45-c713-450f-ad78-84d9615ca7cf.

Acknowledgements

This research was undertaken in the context of MICROMAN project (“Process Fingerprint for Zero-defect Net-shape MICROMANufacturing”, http://www.microman.mek.dtu.dk/). MICROMAN is a European Training Network supported by Horizon 2020, the EU Framework Programme for Research and Innovation (Project ID: 674801). The authors would also gratefully acknowledge the financial support from the EPSRC (EP/K018345/1) for this research.

References

Al-Mashikhi, S.O., Powell, J., Kaplan, A.F.H., Voisey, K.T., 2011. Heat affected zones and oxidation marks in fiber laser-oxygen cutting of mild steel. J. Laser Appl. 23, 1–7. https://doi.org/10.2351/1.3614404.

Cai, Y., Chang, W., Luo, X., Sousa, A.M.L., Lau, K.H.A., Qin, Y., 2018. Superhydrophobic structures on 316L stainless steel surfaces machined by nanosecond pulsed laser. Precis. Eng. 52, 266–275. https://doi.org/10.1016/j.precisioneng.2018.01.004.

Cao, H., Liu, X., Meng, F., Chu, P.K., 2011. Biological actions of silver nanoparticles embedded in titanium controlled by micro-galvanic effects. Biomaterials 32, 693–705. https://doi.org/10.1016/j.biomaterials.2010.09.066.

Cao, P., He, X., Xiao, J., Yuan, C., Bai, X., 2018. Covalent bonding of AgNPs to 304 stainless steel by reduction in situ for antifouling applications. Appl. Surf. Sci. 452, 201–209. https://doi.org/10.1016/j.apsusc.2018.04.227.

Dakal, T.C., Kumar, A., Majumdar, R.S., Yadav, V., 2016. Mechanistic basis of antimicrobial actions of silver nanoparticles. Front. Microbiol. 7, 1–17. https://doi.org/10.3389/fmicb.2016.01831.

De Giglio, E., Cafagna, D., Cometa, S., Allegretta, A., Pedico, A., Giannossa, L.C., Sabbatini, L., Mattioli-Belmonte, M., Iatta, R., 2013. An innovative, easily fabricated, silver nanoparticle-based titanium implant coating: development and analytical characterization. Anal. Bioanal. Chem. 405, 805–816. https://doi.org/10.1007/s00216-012-6293-z.

Diantoro, M., Fitrianingsih, R., Mufti, N., Fuad, A., 2014. Synthesis of silver nanoparticles by chemical reduction at various fraction of MSA and their structure characterization. AIP Conf. Proc. 1589, 257–261. https://doi.org/10.1063/1.4868795.

Dobre, M., Bolle, L., 2002. Practical design of ultrasonic spray devices: experimental testing of several atomizer geometries. Exp. Therm. Fluid Sci. 26, 205–211. https://doi.org/10.1016/S0894-1777(02)00128-0.

Echeverrigaray, F.G., Echeverrigaray, S., Delamare, A.P.L., Wanke, C.H., Figueroa, C.A., Baumvol, I.J.R., Aguzzoli, C., 2016. Antibacterial properties obtained by low-energy silver implantation in stainless steel surfaces. Surf. Coatings Technol. 307, 345–351. https://doi.org/10.1016/j.surfcoat.2016.09.005.

Fazio, E., Santoro, M., Lentini, G., Franco, D., Pietro, S., Guglielmino, P., Neri, F., 2016. Iron oxide nanoparticles prepared by laser ablation: synthesis, structural properties and antimicrobial activity. Colloids Surf. A Physicochem. Eng. Asp. 490, 98–103. https://doi.org/10.1016/j.colsurfa.2015.11.034.

Ferraris, M., Perero, S., Ferraris, S., Miola, M., Vernè, E., Skoglund, S., Blomberg, E., Odnevall Wallinder, I., 2017. Antibacterial silver nanocluster/silica composite coatings on stainless steel. Appl. Surf. Sci. 396, 1546–1555. https://doi.org/10.1016/j.apsusc.2016.11.207.

Ferraris, S., Warchomicka, F., Ramskogler, C., Tortello, M., Cochis, A., Scalia, A., Gautier di Confiengo, G., Keckes, J., Rimondini, L., Spriano, S., 2019. Surface structuring by electron beam for improved soft tissues adhesion and reduced bacterial contamination on Ti-grade 2. J. Mater. Process. Technol. 266, 518–529. https://doi.org/10.1016/j.jmatprotec.2018.11.026.

Gaete-Garretón, L., Briceño-Gutiérrez, D., Vargas-Hernández, Y., Zanelli, C.I., 2018. Ultrasonic atomization of distilled water. J. Acoust. Soc. Am. 144, 222–227. https://doi.org/10.1121/1.5045558.

Gurunathan, S., Han, J.W., Kwon, D.N., Kim, J.H., 2014. Enhanced antibacterial and antibiofilm activities of silver nanoparticles against Gram-negative and Gram-positive bacteria. Nanoscale Res. Lett. 9, 1–17. https://doi.org/10.1186/1556-276X-9-373.

Heinonen, S., Huttunen-saarivirta, E., Nikkanen, J., Raulio, M., Priha, O., Laakso, J., Storgårds, E., Levänen, E., 2014. Antibacterial properties and chemical stability of superhydrophobic silver-containing surface produced by sol – gel route. Colloids Surf. A Physicochem. Eng. Asp. 453, 149–161.

Inoue, Y., Uota, M., Torikai, T., Watari, T., Noda, I., Hotokebuchi, T., Yada, M., 2010. Antibacterial properties of nanostructured silver titanate thin films formed on a titanium plate. J. Biomed. Mater. Res. – Part A 92, 1171–1180. https://doi.org/10.1002/jbm.a.32456.

Jia, Z., Xiu, P., Li, M., Xu, X., Shi, Y., Cheng, Y., Wei, S., Zheng, Y., Xi, T., Cai, H., Liu, Z., 2016. Bioinspired anchoring AgNPs onto micro-nanoporous TiO2 orthopedic coatings: trap-killing of bacteria, surface-regulated osteoblast functions and host responses. Biomaterials 75, 203–222. https://doi.org/10.1016/j.biomaterials.2015.10.035.

Li, W.R., Xie, X.B., Shi, Q.S., Zeng, H.Y., Ou-Yang, Y.S., Chen, Y. Ben, 2010. Antibacterial activity and mechanism of silver nanoparticles on Escherichia coli. Appl. Microbiol. Biotechnol. 85, 1115–1122. https://doi.org/10.1007/s00253-009-2159-5.

Moreno-Couranjou, M., Mauchauffé, R., Bonot, S., Detrembleur, C., Choquet, P., 2018. Anti-biofouling and antibacterial surfaces: via a multicomponent coating deposited from an up-scalable atmospheric-pressure plasma-assisted CVD process. J. Mater. Chem. B 6, 614–623. https://doi.org/10.1039/c7tb02473h.

Pohlman, Reimar, K.S, 1965. Investigation of the Mechanism of Ultrasonic Nebulisation

of Liquid Surfaces With Regard to Technical Applications. West German publisher.
Roca, I., Akova, M., Baquero, F., Carlet, J., Cavaleri, M., Coenen, S., Cohen, J., Findlay, D., Gyssens, I., Heure, O.E., Kahlmeter, G., Kruse, H., Laxminarayan, R., Liébana, E., López-Cerero, L., MacGowan, A., Martins, M., Rodríguez-Baño, J., Rolain, J.M., Segovia, C., Sigauque, B., Taconelli, E., Wellington, E., Vila, J., 2015. The global threat of antimicrobial resistance: science for intervention. New Microbes New Infect. 6, 22–29. https://doi.org/10.1016/j.nmni.2015.02.007.
Šarkovic, D., Babovic, V., 2005. On the statistics of ultrasonically produced water droplets. Zeitschrift fur Naturforsch. – Sect. A J. Phys. Sci. 60, 489–493. https://doi.org/10.1515/zna-2005-0704.
Soloviev, M., Gedanken, A., 2011. Coating a stainless steel plate with silver nanoparticles by the sonochemical method. Ultrason. Sonochem. 18, 356–362. https://doi.org/10.1016/j.ultsonch.2010.06.015.
Sondi, I., Salopek-Sondi, B., 2004. Silver nanoparticles as antimicrobial agent: a case study on E. coli as a model for gram-negative bacteria. J. Colloid Interface Sci. 275, 177–182. https://doi.org/10.1016/j.jcis.2004.02.012.
Stern, K.H., 1972. High temperature properties and decomposition of inorganic salts part 3, nitrates and nitrites. J. Phys. Chem. Ref. Data 1, 747. https://doi.org/10.1063/1.3253104.
Thorslund, T., Kahlen, F., Kar, A., 2003. Temperatures, pressures and stresses during laser shock processing. Opt. Lasers Eng. 39, 51–71.
Tong, S.Y.C., Davis, J.S., Eichenberger, E., Holland, T.L., Fowler, V.G., 2015. Staphylococcus aureus infections: epidemiology, pathophysiology, clinical manifestations, and management. Clin. Microbiol. Rev. 28, 603–661. https://doi.org/10.1128/CMR.00134-14.
Vollmerhausen, T.L., Conneely, A., Bennett, C., Wagner, V.E., Victor, J.C., Byrne, C.P.O., 2017. Visible and UVA light as a potential means of preventing Escherichia coli bio fi lm formation in urine and on materials used in urethral catheters. J. Photochem. Photobiol. B, Biol. 170, 295–303. https://doi.org/10.1016/j.jphotobiol.2017.04.018.
Wang, X., Ma, C., Li, C., Kang, M., Ehmann, K., 2018. Influence of pulse energy on machining characteristics in laser induced plasma micro-machining. J. Mater. Process. Technol. 262, 85–94. https://doi.org/10.1016/j.jmatprotec.2018.06.031.
Zhou, J., Shen, H., Pan, Y., Ding, X., 2016. Experimental study on laser microstructures using long pulse. Opt. Lasers Eng. 78, 113–120. https://doi.org/10.1016/j.optlaseng.2015.10.009.